X-ray microtomography to evaluate the efficacy of paraffin wax coating for soil bulk density evaluation

Luiz F. Pires[a], Sacha J. Mooney[b], André C. Auler[a], Brian Atkinson[b], Craig J. Sturrock[b]

[a] *Laboratory of Physics Applied to Soils and Environmental Sciences, Department of Physics, State University of Ponta Grossa (UEPG), 84.030-900, Ponta Grossa, PR, Brazil*
[b] *Division of Agricultural and Environmental Sciences, School of Biosciences, University of Nottingham, Sutton Bonington Campus, Leicestershire LE12 5RD, UK*

Corresponding author:

Prof. Dr. Luiz F. Pires, Phone: (55) 42-3220-3044. Fax: (55) 42-3220-3042. E-mail: lfpires@uepg.br (L.F. Pires)

Prof. Dr. Sacha J. Mooney. E-mail: sacha.mooney@nottingham.ac.uk

Proofs should be sent to:

Dr. Luiz Fernando Pires, Departamento de Física, Universidade Estadual de Ponta Grossa, Campus de Uvaranas, Bloco L, Sala 15B; Av. Carlos Cavalcanti, 4748, CEP 84.030-900, Ponta Grossa, PR, Brazil.

X-ray microtomography to evaluate the efficacy of paraffin wax coating for soil bulk density evaluation

L.F. Pires[a,1], S.J. Mooney[b,1], A.C. Auler[a], B. Atkinson[b], C.J. Sturrock[b]

[a] *Laboratory of Physics Applied to Soils and Environmental Sciences, Department of Physics, State University of Ponta Grossa (UEPG), 84.030-900, Ponta Grossa, PR, Brazil*

[b] *Division of Agricultural and Environmental Sciences, School of Biosciences, University of Nottingham, Sutton Bonington Campus, Leicestershire LE12 5RD, UK*

ABSTRACT

The paraffin-coated method is a well used approach to measure the soil bulk density (BD). BD is a physical property of great importance for studies of soil quality and health. Therefore, representative measurements of this property are highly valued. Resin and paraffin wax are utilized to coat soil samples however; if these materials ingress into the sample it could affect the representativeness of BD evaluation. The advance in three-dimensional (3D) image analysis techniques such as X-ray microtomography (µCT) offers a great opportunity to visualize and quantify the possible penetration of paraffin wax into clod samples. In this paper we investigated porous system morphological properties of soil samples coated with paraffin wax. The morphological properties of the pores filled with paraffin wax inside the samples were also studied. We observed qualitatively that samples with large pores close to their borders were more susceptible to the penetration of paraffin wax. Samples with pores >10 mm^3 had the highest amount

[1] Corresponding authors.
Tel.: +55 42 3220-3044; Fax: +55 42 3220-3042
E-mail addresses: lfpires@uepg.br (LF Pires); sacha.mooney@nottingham.ac.uk (SJ Mooney)

of paraffin wax into them. Triaxial shaped and complexly pores also offered less resistance to the ingress of paraffin wax. Positive relations between the amount of paraffin wax inside the samples and the volume of pores measured, pore tortuosity and degree of anisotropy were found. Conversely, the soil pore connectivity was not correlated with the penetration of paraffin wax into the samples, at least for the region of interest ($\approx$27.3 cm^3) studied. Finally, an analysis of the impact of paraffin wax ingress inside the samples in measured BD showed increments of $\approx$0.09 and $\approx$0.11 g cm^{-3} in this property when the paraffin wax penetrates into the large pores.

Keywords: X-ray Computed Tomography; Soil porous system; Connectivity; Tortuosity; Soil bulk density.

1. Introduction

Soil bulk density (BD) represents an important physical property obtained by the ratio of mass of solids to the total sample volume. This soil property can be measured by several different methods in wet and dry samples (Hillel, 2004). Soil bulk density is commonly utilized as an index of soil quality and health (Gantzer and Anderson, 2002; Hakansson and Lipiec, 2000), used to convert between weight and volume of soil, and also for water content and soil porosity or pore volumes (Hillel, 2004), and a widely accepted property for referring to the compactness of a soil (Lal and Shukla, 2004).

There are several methods employed to measure BD as described by Grossman and Reinsch (2002) and Shipp and Matelski (1965). The most traditional is the core method, which makes use of cylinders to collect the samples. Timm et al. (2005) and Pires et al. (2011) present a discussion about nuclear and traditional methods for measuring BD. According to these authors, each method has their own particularities and the choice of one over the others depends on several factors, such as, for example, site characteristics, time, laboratory or field measurements and costs.

The paraffin-coated method is another common traditional methodology for measurement of BD (Auler et al., 2017; Grossman and Reinsch, 2002). In this method

the volume of the samples is determined by coating them with a water-repellent substance. Normally, paraffin wax is used due to its low cost and easiness to work with (Holden, 1994). However, the technique is prone to error if the paraffin wax penetrates the pores within the soil sample rather than simply coating its surface (Rossi et al., 2008; Grossman and Reinsch, 2002). In routine measurement, the identification of the paraffin wax penetration inside the clods is not easy and, probably, errors in the measurement of BD through the paraffin-coated method do occur but are unquantifiable. If paraffin does ingress into a soil sample, the impact on measurement of BD by this method could be significant.

According to van Remortel and Shields (1993), the ingress of paraffin wax into soil clods can reduce their measured volume and, consequently, it results in a higher BD (Solgi et al., 2018). For very gravely soils, Hirmas and Furquim (2006) observed that when the paraffin wax is absorbed deep into clods, problems to remove the soil and wax coatings on the gravel tend to inflate the mass of gravel. Therefore, the mass of gravel in clod samples is overestimated increasing BD (Rossi et al., 2008).

Methods of image analysis such as X-ray Computed Tomography (CT), which is based on the attenuation of the radiation by materials of different densities (Pires, 2018), can assess the internal structure of soil samples and potentially quantify the penetration of paraffin wax. Since the development of the X-ray CT in the early seventies of the last century (Hounsfield, 1973), many applications of this technique have been applied across different research areas, where the aim was to study the internal structure of porous media (Ferreira et al., 2018; Carducci et al., 2017; Cnudde and Boone, 2013; Mooney et al., 2012; Vaz et al. 2011; Pires et al., 2010; Crestana et al., 1985). The combination of the X-ray CT data and image analysis programs permits a detailed 3D characterization of the soil porous system (Grayling et al., 2018; Tseng et al., 2018; Borges et al., 2018; San José Martinez et al., 2017; Luo et al., 2010). Morphological

76 measurements such as pore volume, shape, orientation, continuity, tortuosity and

77 macropore size distribution can be obtained from X-ray CT images.

78 No previous study has sought to quantify the potential ingress of paraffin wax

79 inside soil samples. The objective of this study was to investigate the possibility of

80 paraffin wax penetration inside soil samples and to study the effect of the pore

81 morphological properties on the amount and distribution of paraffin wax within the

82 samples. These objectives were achieved through 3D X-ray CT analysis of samples

83 coated with paraffin wax at the resolution scale of mesopores and macropores.

84 ## 2. Materials and methods

85 *2.1 Sample characteristics and preparation*

86 Samples were collected from the experimental farm of the Agricultural Research

87 Institute of Parana (IAPAR) in the city of Ponta Grossa, PR, Brazil (25°06'S, 50°10'W,

88 875 m above sea level). The soil under investigation was an Oxisol (Rhodic Hapludox),

89 according to USDA soil taxonomy (Soil Survey Staff, 2013), of clay texture (17% sand,

90 22% silt, and 61% clay).

91 Three sets of samples were collected for this study: Group 1 – samples with

92 volumes between 50 and 100 cm^3, which were utilized for BD measurement by the

93 paraffin-coated method (n=8 samples); Group 2 – samples with volumes between 90

94 and 97 cm^3, which were utilized for BD measurement by the core and paraffin-coated

95 methods (n=14 samples); and Group 3 – samples with volumes ranging from 70 to 75

96 cm^3, which were employed for the image analysis (n=36 samples). All the samples were

97 manually collected at the soil surface (0-10 cm) with the help of an Uhland sampler (core

98 method – stainless steel cylinders with height of ≈5.0 cm and internal diameter of ≈4.8

99 cm) and shovel and trowel (clod method). Samples of groups 1 and 2 were collected in

100 August 2018 and of group 3 in April 2017. An area of about 3.0 to 3.0 m under minimum

101 tillage was selected to collect the samples near the center of the experimental plot (50 ×

102 120 m) for groups 1 to 3. A distance of around 20 to 30 cm was kept between samples

103 throughout the sampling procedures, which were carried out after harvest (normally

104 ryegrass – *Lolium multiflorium*).

105   The samples of group 1 were selected to measure the impact of the paraffin wax

106 ingress in direct measurements of BD by the paraffin-coated method, while the samples

107 of group 2 were chosen to show the differences in BD before and after coating with

108 paraffin wax. The samples of group 2 were carefully removed from the cylinders prior the

109 coating procedure. These samples were also analyzed to identify possible differences in

110 BD caused by soil spatial variability, instead by the paraffin wax penetration. The ingress

111 of paraffin wax into the samples of groups 1 and 2 was verified based on visual

112 examination after disintegrating the samples (Fig. 1d). Finally, samples of group 3, which

113 were also carefully extracted from cylinders, were analyzed to investigate, through image

114 analysis, the effect of pore morphological properties on the amount and distribution of

115 paraffin wax inside the soil samples. Prior to X-ray CT scanning, samples were dried at

116 40 ºC until their mass became constant, in order to eliminate as much of the water phase

117 as possible from the samples (Jefferies et al., 2014).

118   For the impregnation of the samples, hard paraffin wax was kept in a container

119 and melted until air bubbles were no longer observed. The temperature was controlled

120 with a digital LCD thermometer (Figs. 1a,b). Carefully a piece of thread (nylon string)

121 was tied around the sample, leaving about 15 cm free. Holding onto the end of the free

122 thread, the sample was momentarily dipped in the melted paraffin wax. The excess of

123 paraffin wax was allowed to drain after the previous step. The next step was to wait for

124 the adhering paraffin wax to solidify (~10 minutes). This procedure was carried out

125 individually for each soil sample studied.

126   The BD measurement by the core method was made following the procedures

127 described in Grossman and Reinsch (2002). For the paraffin-coated method, first the

128 weight of the soil clod (W_1) was measured in air and again after coating with paraffin wax

129   (W_2). The weight of paraffin-wax used in coating was obtained by the difference between

130   W_2 and W_1. The total clod volume coated with paraffin wax (V_t) was measured after

131   weighting the clod submerged in water. The volume of paraffin wax utilized in coating

132   (V_{pa}) was determined using the weight of paraffin wax employed in coating and its density

133   (0.90 g cm^{-3}). Finally, the actual volume of soil (V_s) was calculated by the difference

134   between V_t and V_{pa}, and, BD as the ratio of W_1 and V_s.

135   *2.2 X-ray Computed Tomography*

136   Each soil sample was scanned using a GE v|tome|x m X-ray CT scanner (GE

137   Measurement & Control Solutions, Wunstorf, Germany) at the Hounsfield Facility (The

138   University of Nottingham, Sutton Bonington Campus, UK). The voltage, current and

139   integration time adopted for the image acquisition process were 180 kV, 160 µA and 250

140   ms. A 0.1 mm Cu-filter was used to minimize beam-hardening effects. A total of 2520

141   projections were obtained per sample with a pixel resolution of 35 µm. Therefore, it was

142   not possible to resolve pores below this resolution.

143   *2.3 Image reconstruction, processing and analysis*

144   The radiographs of each scan were reconstructed in 32 bit format in order to avoid

145   compression of the greyscale histogram. After reconstruction the images were imported

146   into Volumetric Graphics (VG) StudioMAX® 2.0 and after into ImageJ 1.42 and cropped

147   to a cubic shape with $30.1 \times 30.1 \times 30.1$ mm^3 ($860 \times 860 \times 860$ pixels).

148   The main objective of the image analysis was the verification of the possibility of

149   paraffin wax penetration into the soil samples after the coating procedure. After that,

150   some morphological properties of the soil porous system was measured with an aim to

151   evaluate the influence of them in the paraffin wax penetration into the samples. The

152   choice of a region of interest smaller than the whole soil sample imaged was based on

153   the time needed for each image analysis (several days) and the computational work. The

154   amount of computer system memory (64 GB RAM) allocated for the analyses allowed

155   only to work with samples of size similar to the region of interest selected. The complexity

156   of the soil porous system and the number of parameters studied influenced the amount

157   of memory necessary for the measurements. However, the volume of the samples

158   (region of interest) analyzed were selected close to the borders of them. This was made

159   due to the importance of the pores next to the sample surface to the entrance of paraffin

160   wax. However, we believe that the use of special masks (image analysis procedures)

161   and powerful computers can allow the future analysis of entire and big volumes for a

162   better characterization of the soil porous system and it susceptibility to the paraffin wax

163   ingress.

164   A preliminary analysis revealed that 27 of the 36 samples had negligible paraffin

165   wax ingression. As such no further analysis was conducted on these samples. A full

166   morphological characterization was subsequently performed on the remaining nine

167   samples (25%) for the region of interest selected. So, we decided to call these samples

168   in the text as S1 to S9.

169   The original grey-level X-ray CT images were processed using ImageJ 1.42

170   software (Rasband, 2007). The segmentation process was based on the nonparametric

171   and unsupervised Otsu method of threshold (Otsu, 1979). The images were also visually

172   inspected to verify the quality of the segmentation procedure. This resulted in a binary

173   image, in which pores and soil material were respectively represented by white and black

174   pixels. A third peak was also observed in the image cross sections, which was related to

175   the paraffin wax (Fig. 2). The threshold value defined based on the Otsu method was the

176   same for all the cross sections of a same sample. To segment the paraffin wax only by

177   the Otsu method, image tools such as subtract background (radius 350 pixels), enhance

178   contrast (0.5%), remove outliers (radius 0.7 pixels) and median 3D filters (radius 2.0

179   pixels) were utilized. After this procedure a binary image of the pores filled with paraffin

180   wax in black and the solid phase in white pixels was obtained. In these images, pores

181   not filled with paraffin were disregarded.

182   For the 3D structural assessment, soil pores were classified according to their

183 size and shape distribution. For the shape classification, geometrical parameters known

184 as major, intermediate and minor axes of the ellipsoids that represent each pore were

185 determined by using 3D measuring techniques (Schmitt et al., 2016; Bullock et al., 1985).

186 These parameters were measured using the Particle Analyser tool in ImageJ. Binary

187 images of the whole soil porous system and the pores filled only with paraffin wax were

188 utilized in these measurements. Isolated pores <9 voxels were removed from the porous

189 fraction of the images in the quantitative analyses to avoid misclassification from

190 unresolved voxels (Jefferies et al., 2014). The soil pores which allowed the measurement

191 of the three principal axes were classified according to the terminology suggested by

192 Zingg (1935). The relation between the ratio of the intermediate by the major (Int./Maj.)

193 axis and the ratio of the minor by the intermediate (Min./Int.) axis allows the classification

194 of pores based on shape. Therefore, the pores were classified as: Equant (EQ), Prolate

195 (PR), Oblate (OB), and Triaxial (TR) (Pires et al., 2017). When one of the axes of a

196 specific pore could not be determined, this pore was not classified (unclassified pore)

197 according to its shape. These pores are associated enhanced complexity of individual

198 pores, which means that a geometrical shape cannot be fitted for them.

199   The porosity (P) and number of pores (NP) were calculated taking into

200 consideration the resolvable pores. In this study the term porosity refers to the sum of

201 mesopores and macropores based on the size classification of Brewer (1964). The pore

202 size distribution (sorted by pore volume) corresponded to the total number of

203 disconnected pore volumes inside the sample. For P and NP size distribution analysis,

204 pores were classified in different volume intervals: 0.0001-0.01; 0.01-0.1; 0.1-1; 1-10;

205 and >10 mm^3. These volume intervals were selected based on the importance of different

206 pore sizes in the water infiltration, redistribution, retention and root penetration, for

207 instance.

208   The X-ray CT images were also analyzed in terms of network tortuosity (τ) and

209   connectivity of the pores using the Osteoimage software (Roque et al., 2009). The

210   tortuosity, which is geometrically defined by the ratio between the geodesic distance

211   between two connected points and the Euclidian distance between these two points, was

212   calculated through the geodesic reconstruction algorithm (Roque et al., 2012a,b). The

213   Characteristic of Euler-Poincaré (EPC) was utilized to estimate the degree of

214   connectivity, which represents one of the Minkowski functions and a topological measure

215   used for describing the connectivity of spatial structures (Katuwal et al., 2015). EPC per

216   sample volume was obtained considering 859 disectors, which represent contiguous

217   image sections. EPC was estimated based on the algorithm discussed in Vogel and

218   Kretzshmar (1996) from a set of sequential 2D registered images by the use of the

219   dissector, which consists of two parallel sections a small distance apart. The dissector

220   displacement in our case studies was 0.035 mm, thus pores that lay in between the

221   image slices could not be considered as they did not contribute according to the

222   morphological operations (erosion and dilation by one pixel) implemented in the

223   algorithm for the stereological procedures, which eliminates pores lesser than ≈0.0007

224   mm^3. Therefore, a sizeable volume of the isolated pores is not considered by this

225   approach. In our study the volumetric EPC ($EPC_V = EPC/V$), i.e., by the volume of

226   dissectors, was determined after the images had been previously submitted to the Purify

227   procedure in Bone J plugin (Odgaard and Gundersen, 1993; Toriwaki and Yonekura,

228   2002). The EPC_V number is an indicator of how well connected is a pore: the smaller

229   (more negative) it is, the higher is the pore connectivity (Chappard et al., 1999; Roque

230   et al., 2009).

231   The Euler Number (EN) was also utilized to evaluate the connectivity of pores

232   larger than 0.2 mm^3 ($EN_{>0.2}$) and the largest pore (EN_B) found. EN was evaluated using

233   the Particle Analyser and Bone J plugins in ImageJ, which allowed the analysis of

234   connectivity of individual pores of different volumes (Doube et al., 2010). Prior the EN

235   analyses, the image stacks were also submitted to the Purify procedure in Bone J plugin

236   as done for EPC_V.

237   Parameters such as porosity, number of pores, and pore volume (PV) were also

238   obtained for pores larger than 0.2 mm^3. This analysis was carried out for the whole soil

239   porous architecture and for the pores filled only with paraffin wax. The degree of

240   anisotropy (DA), which gives the preferred orientation of pores, was also determined in

241   3D by using the Bone J plugin.

242   Statistical analyses were performed with the Past program (Hammer et al., 2001).

243   Pearson correlations among each pair of variables were measured for the entire

244   set of morphological parameters. The t-test ($p \leq 0.05$) was used to compare the effect of

245   paraffin wax ingress in BD measurements.

246   **3. Results and discussion**

247   *3.1 Image analysis*

248   3D images of the sample S8 are shown in Fig. 2. It is possible to observe in the

249   images the penetration of paraffin wax inside the sample due to the procedure of coating.

250   A qualitative analysis of the images also demonstrates that the largest pores at the

251   sample surface were filled with paraffin wax, which is expected due to the reduced

252   energy, solid-liquid contact angles, required to fill these pores (Jury and Horton, 2004;

253   Or and Wraith, 2002).

254   Some authors have reported that the materials (resin or paraffin wax) utilized to

255   coat the samples may not adequately seal the deepest pores, which can allow water

256   penetration into them, affecting the measurement of their volumes (Sander and Gerke,

257   2007). On the other hand, the complete coating of soil samples with these characteristics

258   could lead to the resin/paraffin penetration into them, as observed in our study. In

259   addition to the influence of resin/paraffin entrance into the samples in the measurement

260   of BD, this problem can also influence the measurement of other physical properties

261 such as water content and shrinkage curve measurements (Stewart et al., 2012; Schafer

262 and Singer, 1976).

263 *3.2 Morphological physical properties*

264 Sample S6 was characterized by the smallest porosity and pore volume (P:

265 10.9% and PV: 2976) and S8 by the highest (P: 23.7% and PV: 6452), which indicates

266 the relative variability (CV: 24.8% and CI: 3.0 for P; CV: 25.8% and CI: 846 for PV) of

267 these properties among samples (Figs. 3a,b). The terms CV and CI stand for coefficient

268 of variation and confidence interval (95%), respectively. In terms of NP (Fig. 3c), the

269 smallest value was for S3 (50921) and the highest for S4 (68774). In general, the

270 samples with the highest P and PV had the largest volume of paraffin wax inside them

271 (Table 1) and they were characterized by the presence of larger pores ($NP_{>0.2}$), which

272 had a great contribution to P (Fig. 4a and Table 2).

273 The volumetric Euler-Poincare Characteristic (Fig. 3d), a measurement of the

274 connectivity of the pores (Chappard et al., 1999), was lower for S7 (-0.0118 mm^{-3}) and

275 higher for S6 (-0.0030 mm^{-3}). As discussed earlier the smaller EPC_V, the higher the pore

276 connectivity (Roque et al., 2009). The pore size distribution analysis (Fig. 4a) showed

277 that large pores contributed to more than 90% of P (Table 2). For example, the samples

278 with the largest proportion of paraffin wax inside them (S5, S8, S9) had more than 82%

279 of their pores >0.2 mm^3 filled with paraffin (Tables 3 and 4). Therefore, the Euler Number,

280 a measure of the degree of fragmentation of the pore networks (Schmitt et al., 2016),

281 was undertaken for pores >0.2 mm^3 (Table 2). The pore network was less connected for

282 S6 (-92183) and high connected for S1 (-248844). As observed for EPC_V (r=0.31), there

283 was no significant relation between the pore connectivity results and the amount of

284 paraffin wax inside the samples (Table 1). The presence of main, connected pore

285 networks would be expected to contribute to a more effective flow path, but this was not

286 observed in terms of paraffin wax penetration inside the samples for the region of interest

287 studied (Rezanezhad et al., 2009). Differences in the chemical-physical properties of the

288   paraffin wax (for example, surface tension, density, viscosity) in comparison to water and

289   the presence of small pores connecting parts of the main pore network might account for

290   this unexpected result (Lal and Shukla, 2004; Hillel, 2004; Turner et al., 1955). The

291   possibility of the analysis of the whole sample studied, which means to characterize the

292   pores in the border of the samples, could complement the results obtained and, perhaps

293   show some different relation between the amount of paraffin wax and connectivity.

294   However, it was not possible to analyze in our study the morphological properties of the

295   entire sample as earlier discussed.

296   The smallest tortuosity was measured for S6 (1.05) and the highest for S8 (1.14)

297   (Fig. 3e). High values of τ are normally related to a more disconnected network

298   (Rezanezhad et al., 2009). Samples with the largest amount of paraffin (S5, S8, S9) were

299   also those with the largest τ (Tables 1 and 3). However, the small values of τ indicate

300   that there was no significant fragmentation of the mesopores and macropores, which is

301   in line mainly with the results of $EN_{>0.2}$ (Katuwal et al., 2015; Pagenkemper et al., 2014).

302   The degree of anisotropy results indicate an isotropic soil porous system (Fig. 3f).

303   Small values of DA, close to 0, suggest a soil porous system that is isotropic and water

304   infiltration tends to be vertical. Values close to 1 suggest that the soil porous system is

305   anisotropic and water infiltration can occur parallel to the soil surface (Tseng et al., 2018).

306   The smallest DA value was in S4 (0.08) and the highest for S1 (0.27). In general, the

307   samples with the largest amount of paraffin wax inside them were also those with the

308   highest DA values (Table 1). However, the DA results should be used with caution in our

309   work because the soil dipped into the melted paraffin wax is subjected to flow from

310   different directions. The idea behind these results was try to find some relation between

311   the isotropy of the soil porous system and the possibility of paraffin wax ingress into the

312   samples.

313   *3.3 Pore size and shape distribution (whole porous system)*

314   The volume of pores and their contribution to P considering the regions of the

315   porous space occupied with paraffin wax are presented in Table 3. Samples S5, S8 and

316   S9 were characterized by the largest amount of paraffin wax inside them. More than 40%

317   of this subset of samples (S1 to S9) had >20% of their volumes filled with paraffin wax,

318   which can affect the representativeness of sample volume or bulk density evaluation

319   (Grossman and Reinsch, 2002; Russell and Balcerek, 1944). The presence of cracks

320   and macropores can contribute to the penetration of paraffin wax (Casanova et al., 2016;

321   Gonçalves et al., 2013; Sander and Gerke, 2007; Page-Dumroese et al., 1999; Schafer

322   and Singer, 1976).

323   To further consider the influence of the soil sample structure in the penetration of

324   paraffin wax, 3D pore size and shape distribution measurements were undertaken (Fig.

325   4). Values of normalized average P, PV and NP, as a function of the shape and size of

326   the pores, were obtained for the nine samples (S1 to S9) studied. It was observed in

327   each case that a single largest pore (>10 mm^3) made the highest contribution to P, which

328   varied from around ≈92% (S6) to ≈97% (S8) (Fig. 4a). In relation to NP, the largest

329   number of pores was within the range of 0.0001 to 0.01 mm^3, which varied from ≈93%

330   (S6) to ≈97% (S1) (Fig. 4b). Similar results were also observed in similar studies for

331   Brazilian tropical soils (Ferreira et al., 2018; Passoni et al., 2015).

332   The PV and NP variation patterns (results not showed in the paper) in terms of

333   shape were similar among samples (S1 to S9) (Figs. 4c-f). The largest contribution to

334   PV was from the unclassified pores, from ≈54% (S1) to ≈66% (S4), while the smallest

335   was for equant (S4: ≈3%; S1: ≈6%) and oblate (S4: ≈5%; S7: ≈6%) shaped pores (Fig.

336   4c). The same tendency was observed for NP, which demonstrates the relation between

337   PV and NP (Fig. 4d). In summary, the unclassified pores contributed to ≈61% of PV and

338   ≈77% of NP followed by the triaxial shaped pores (PV: ≈21% and NP: ≈10%) (Figs. 4c,d).

339   When the unclassified pores were not considered in the analysis (Figs. 4e,f), the

340   largest contribution to PV was for the triaxial shaped pores from ≈49% (S1) to ≈58% (S3),

341   while the smallest was for equant (S6: ≈8%; S1: ≈13%) (Fig. 4e). The objective of

342   excluding unclassified pores was to ensure the evaluation was only for those pores

343   classified by the shape index where paraffin wax ingress had taken place. The same

344   tendency was observed for NP, which demonstrates the relation between PV and NP

345   (Fig. 4f).

346   It is important to note that triaxial (laminar), oblate (disk) and prolate (channel)

347   pores have elongated shapes while equant are spheroidal (Bullock et al., 1985). Cracks

348   and thin fissures are usually associated with elongated pores, whereas fauna activity

349   and trapped air is associated with the spherical ones (Pagliai, 1984). As described early,

350   a large proportion of the pore space (≈77% among samples) in this study were not

351   classified in terms of shape due to the extent of their complexity (Tseng et al., 2018;

352   Pires et al, 2017). Nevertheless, we noted that the pore size and shape distribution

353   results cannot completely explain the differences observed in the amount of paraffin wax

354   in the samples (Table 3). Therefore, a further analysis of the pore size and shape

355   distribution was performed considering only the regions of the sample pore space filled

356   with paraffin wax.

357   *3.4 Pore size and shape distribution (regions filled with paraffin)*

358   In terms of pore size distribution, the largest contribution to P was found for the

359   single, largest pore (>10 mm^3), similar to the results of the whole soil porous system (Fig.

360   4a). Exceptions were S3 and S4 (results not showed in the paper), which had

361   contributions of ≈27% and ≈20% for these pore sizes (Fig. 4a). The samples with the

362   highest contributions were S5 (≈83%), S8 (≈96%), and S9 (≈95%). In general, the

363   samples with the largest contribution of large pores to P were also those with the highest

364   amount of paraffin wax inside them (r=0.68, p<0.05) (Tables 1 and 3). Sample S7 was

365   an exception (results not showed in the paper), as it was characterized by the highest

366   NP (≈93%) in the region of sizes of 0.1 to 1.0 mm^3 (Fig. 4b). As observed for the

367   contribution of large pores to P, in general, samples with the highest NP for pore sizes

368 >1 mm^3 (S5: ≈19%; S8: ≈24%; S9: ≈22%) were also those with the largest amount of

369 paraffin wax inside them (Figs. 4a,b). Large pores are very important and their key

370 function in the soil porous system is to facilitate the movement of air and drainage of

371 solutes (Lal and Shukla, 2004). Therefore, less energy is required to fill these pores with

372 paraffin wax (Kutílek and Nielsen, 1994).

373   For pore shape, the largest and the smallest contribution to PV and NP was again

374 observed for pores unclassified in terms of shape (PV: ≈86% and NP: ≈74%) (Figs. 4c,d).

375 This was expected because the largest amount of paraffin wax ingressed inside the soil

376 samples was found in the largest pores, which are characterized by their complexity (Fig.

377 2).

378   When pores not classified in terms of their shape were excluded, the largest and

379 the smallest contribution to PV was observed for triaxial (S3: ≈55%; S4: ≈93%) and

380 equant (S1: ≈0%; S6: ≈3%) shaped pores (Fig. 4e). The same tendency was verified for

381 NP (S3: ≈65%; S4: ≈87% for triaxial and S1: ≈0%; S8: ≈4% for equant) (Fig. 4f).

382 However, as observed in Fig. 4c, the largest proportion of pore volumes (≈86%) filled

383 with paraffin wax was verified for the unclassified pores in terms of shape. A strong

384 positive correlation (r=0.72, p<0.05) was measured between the volume of paraffin wax

385 inside the samples and the percentage of unclassified pores. This means that the paraffin

386 wax tends to penetrate in the largest pores, which are also more complex. Similar to the

387 results for the whole soil porous system, there was a clear relationship between PV and

388 NP for the pores classified in terms of shape. This suggests pores of triaxial shape offer

389 less resistance to be filled with paraffin wax than the other shapes. Normally, this pore

390 shape is associated with fissures in the samples. In general, the samples with the largest

391 proportion of paraffin wax (S5, S6, S8) were also characterized by the most abundant

392 proportion of oblate and triaxial pore shapes (unclassified pores not included) in terms

393 of PV (r=0.56, p=0.15, S9 not included) (Fig. 4e). An exception was observed for S9,

394 which presented ≈31% of PV due to prolate shaped pores (results not showed in the

395   paper). For NP (Fig. 4f), S4 followed by S9, S8 and S5 presented the largest proportions

396   of the contribution of triaxial shaped pores to NP (S4: ≈87%; S9: ≈77%; S8: ≈72%; S5:

397   ≈71%). However, there was no a clear relation between the amount of paraffin wax inside

398   the samples and NP (r=-0.04).

399   *3.5 Soil bulk density measurement*

400   To evaluate the effect of the paraffin wax into the soil samples in BD

401   measurements we selected two groups of samples. The first (group 1) were clods

402   collected to evaluate the influence of the paraffin wax ingress when the paraffin-coated

403   method is used. The results show that the entrance of paraffin wax into the samples of

404   group 1 presented significant (p≤0.05) changes in BD (Table 5). An increase of around

405   0.11 g cm^{-3} was measured in BD after the entrance of paraffin wax. Different from

406   samples from group 3, the paraffin wax ingress into the soil samples from groups 1 and

407   2 were verified based on the visual examination and not by image analysis.

408   In order to verify that the BD increase was not influenced by the soil spatial

409   variability, we also carried out measurements of BD by the core method (samples of

410   group 2). These samples were later carefully removed from the stainless cylinders for

411   coating with paraffin wax. A reduction of around 25 cm^3 in the volume of the samples

412   analyzed was verified after their removal from the cylinders, which significantly increased

413   (p≤0.05) their BD (Table 5). However, when the same set of samples (group 2) was

414   analyzed by the core method before coating, no significant (p≤0.05) differences were

415   observed in the average BD (1.04 g cm^{-3} – samples with no paraffin wax ingress and

416   1.03 g cm^{-3} – samples with paraffin wax ingress after coating), which means that the

417   differences were caused by the ingress of paraffin wax inside the soil samples (Figs. 1d

418   and 2) and not by their spatial variability. According to van Remortel and Shields (1993),

419   the ingress of paraffin wax into soil clods can reduce their measured volume, and,

420   consequently it results in a higher BD as observed in our results (Solgi et al., 2018).

421   The differences observed in BD from samples from groups 1 and 2 (Table 5) are

422   because clod samples normally overestimates BD from 0.07 to 0.22 g cm^{-3} in relation to

423   core samples, as has been previously shown in the literature (Solgi et al., 2018;

424   Casanova et al., 2016; Gonçalves et al., 2013; Timm et al., 2005; van Remortel and

425   Shields, 1993; Blake and Hartge, 1986). This is based on the tendency of clods collected

426   to exclude pores between structural units. However, our results show that this

427   overestimation could be greater if paraffin wax penetrates into the samples during

428   coating as observed for samples of group 2 (Table 5). This result certainly depends on

429   the characteristics of the soil studied, however, similar findings were observed by Auler

430   et al. (2017) working with another Brazilian Oxisol.

431   An analysis of the image cross-sections revealed the samples with the largest

432   amount of ingressed paraffin wax had a considerable number of large pores close to

433   their borders (Fig. 2). This analysis was mainly based on visual analysis of the X-ray CT

434   images. This result means that samples with these characteristics are more susceptible

435   to paraffin wax penetration. To avoid this problem one suggestion might be to check the

436   quality of the aggregates before coating. Aggregates with a strong grade structure (well-

437   formed and durable) certainly have the smaller probability of paraffin wax be absorbed

438   deep into them than poorly formed and nondurable ones (Hirmas and Furquim, 2006;

439   Hillel, 2004). However, another possibility would be to increase the number of replicates

440   to minimize the influence of this problem. For instance, in this study we used a great

441   number of samples (n=36) and 75% of the coated samples did not present significant

442   ingress of paraffin wax deep into them.

Conclusions

444   The use of X-ray CT allowed us to verify the influence of different soil

445   morphological parameters (shape of pores, pore size distribution, porosity, number of

446   pores, connectivity, tortuosity and degree of anisotropy) in the amount of paraffin wax

447   ingress inside soil samples. We found positive correlations between the amount of

448 paraffin wax into the samples and their pore volume, tortuosity and degree of anisotropy

449 for the region of interest analyzed. Contrary to our expectation, no relation was found

450 between the volume of paraffin wax inside the samples and the porous system

451 connectivity, which can be associated with the volume studied by image analysis. Our

452 results showed that the samples with the largest contribution of large pores to porosity

453 were also those with the highest amount of paraffin wax inside them. The analysis of the

454 pores classified in terms of shape suggested that those with moderately to very flat and

455 moderately to very elongate shapes (triaxial shaped pores) had the greatest influence in

456 the ingress of paraffin wax into the samples. However, the largest pores, which were not

457 classified in terms of shape, had the great influence in the penetration of paraffin wax

458 inside the samples. For the soil samples analyzed, the soil bulk density was increased,

459 when the paraffin wax penetration into the samples was observed. This result is

460 associated to the lowering of the actual volume of the soil due to the ingress of paraffin

461 wax in the clod method used in this work. Thus, we have shown the paraffin-coated

462 method is prone to problems in measurements of soil bulk density due to the paraffin

463 wax penetration, though it does not apply to all soils and with careful selection of samples

464 and increased replication the impact could be minimized.

465 Acknowledgments

References

Auler, A.C., Pires, L.F., Brinatti, A.M., Saab, S.C., 2017. Soil aggregates bulk density: The use of Jolly balance in experimental physics classes for soil science education. Rev. Bras. Ens. Física, 39, e1506-1–e1506-8.

Blake, G.R., Hartge, K.H., 1986. Bulk density, in: Klute, A. (Ed.), Methods of Soil Analysis, Part 1: Physical and Mineralogical Methods, Soil Science Society of America, Madison, WI, pp. 363–382.

Borges, J.A.R., Pires, L.F., Cássaro, F.A.M., Roque, W.L., Heck, R.J., Rosa, J.A., Wolf, F., 2018. X-ray microtomography analysis of representative elementary volume (REV) of soil morphological and geometrical properties. Soil Tillage Res. 182, 112–122.

Brewer, R., 1964. Fabric and mineral analysis of soils. New York: Wiley.

Bullock, N., Fedoroff, A., Jongerius, A., Stoops, G., Tursina, T., 1985. Handbook for Soil Thin Section Description, 1st ed. Waine Research, England.

Carducci, C.E., Zinn, Y.L., Rossoni, D.F., Heck, R.J., Oliveira, G.C., 2017. Visual analysis and X-ray computed tomography for assessing the spatial variability of soil structure in a cultivated Oxisol. Soil Tillage Res. 173, 15–23.

Casanova, M., Tapia, E., Seguel, O., Salazar, O., 2016. Direct measurement and prediction of bulk density on alluvial soils of central Chile. Chilean J. Agric. Res. 76, 105–113.

Chappard, D., Legrand, E., Pascaretti, C., Baslé, M.F., Audran, M., 1999. Comparison of eight histomorphometric methods for measuring trabecular bone architecture by image analysis on histological sections. Microsc. Res. Tech. 45, 303–312.

Cnudde, V., Boone, M.N., 2013. High-resolution X-ray computed tomography in geosciences: A review of the current technology and applications. Earth-Sci. Rev. 123, 1–17.

499   Crestana, S., Mascarenhas, S., Pozzi-Mucelli, R.S., 1985. Static And Dynamic 3

500   Dimensional Studies Of Water In Soil Using Computed Tomographic Scanning. Soil

501   Sci. 140, 326–332.

502   Doube, M., Kłosowski, M.M., Arganda-Carreras, I., Cordelières, F.P., Dougherty, R.P.,

503   Jackson, J.S., Schmid, B., Hutchinson, J.R., Shefelbine, S.J., 2010. BoneJ: Free and

504   extensible bone image analysis in ImageJ. Bone 47, 1076–1079.

505   Ferreira, T.R., Pires, L.F., Wildenschild, D., Heck, R.J., Antonino, A.C.D., 2018. X-ray

506   microtomography analysis of lime application effects on soil porous system.

507   Geoderma 324, 119–130.

508   Gantzer, C.J., Anderson, S.H., 2002. Computed tomographic measurement of

509   macroporosity in chisel-disk and no-tillage seedbeds. Soil Till. Res. 64, 101–111.

510   Gonçalves, F.C., Marasca, I., de Souza, S.F.G., Tavares, L.A.F., Silva, P.R.A., 2013.

511   Métodos de determinação da densidade do solo em diferentes sistemas de manejo.

512   Energ. Agric. 28, 165–169.

513   Grayling, K.M., Young, S.D., Roberts, C.J., de Heer, M.I., Shirley, I.M., Sturrock, C.J.,

514   Mooney, S.J., 2018. The application of X-ray micro Computed Tomography imaging

515   for tracing particle movement in soil. Geoderma 321, 8–14.

516   Grossman, R.B., Reinsch, T.G., 2002. Water retention and storage, in: Dane, J.H., Topp,

517   G.C. (Eds.), Methods of Soil Analysis. Part 4: Physical Methods. Soil Science Society

518   of America, Madison, WI, pp. 201–228.

519   Håkansson, I., Lipiec, J., 2000. A review of the usefulness of relative bulk density values

520   in studies of soil structure and compaction. Soil Till. Res. 53, 71–85.

521   Hammer, Ø., Harper, D.A.T., Ryan, P.D., 2001. PAST: Paleontological statistics software

522   package for education and data analysis. Palaeont. Elect. 4, 1–9.

523   Hillel, D., 2004. Introduction to Environmental Soil Physics. Elsevier Academic Press,

524   Burlington, Massachusetts, USA.

525   Hirmas, D.R., Furquim, S.A.C., 2006. Simple modification of the clod method for

526   determining bulk density of very gravelly soils. Commun. Soil Sci. Plan. 37, 899–906.

527   Holden, N.M., 1994. A rapid method for the visualisation of soil macropores. Plant Soil

528   166, 291–294.

529   Hounsfield, G.N., 1973. Computerized transverse axial scanning (tomography): I.

530   Description of system. Br. J. Radiol. 46, 1016–1022.

531   Jefferies, D.A., Heck, R.J., Thevathasan, N. V., Gordon, A.M., 2014. Characterizing soil

532   surface structure in a temperate tree-based intercropping system using X-ray

533   computed tomography. Agrofor. Syst. 88, 645–656.

534   Jury, W.A., Horton, R.C.N., 2004. Soil physics, 6th ed. John Wiley, Hoboken, NJ, USA.

535   Katuwal, S., Norgaard, T., Moldrup, P., Lamandé, M., Wildenschild, D., de Jonge, L.W.,

536   2015. Linking air and water transport in intact soils to macropore characteristics

537   inferred from X-ray computed tomography. Geoderma 237/238, 9–20.

538   Kutílek, M., Nielsen, D.R., 1994. Soil Hydrology. Catena Verlag, Germany.

539   Lal, R., Shukla, M.K., 2004. Principles of Soil Physics. CRC Press, New York, NY, USA.

540   Luo, L.F., Lin, H., Li, S.C., 2010. Quantification of 3-D soil macropore networks in

541   different soil types and land uses using computed tomography. J. Hydrol. 393, 53–64.

542   Mooney, S.J., Pridmore, T.P., Helliwell, J., Bennett, M.J., 2012. Developing X-ray

543   Computed Tomography to non-invasively image 3-D root systems architecture in soil.

544   Plant Soil 352, 1–22.

545   Odgaard, A., Gundersen, H.J.G., 1993. Quantification of connectivity in cancellous bone,

546   with special emphasis on 3-D reconstructions. Bone 14, 173–182.

547   Or, D., Wraith, J.M., 2002. Soil water content and water potential relationships, in:

548   Warrick, A.W. (Ed.), Soil Physics Companion, CRC Press, Boca Raton, pp. 49–84.

549   Otsu, N., 1979. A threshold selection method from gray-level histograms. IEEE

550   Transactions on Systems, Man and Cybernetics l. SMC-9, 62–6.

551   Page-Dumroese, D.S., Jurgensen, M.F., Brown, R.E., Mroz, G.D., 1999. Comparison of

552   methods for determining bulk densities of rocky forest soils. Soil Sci. Soc. Am. J. 63,

553   379–383.

554   Pagenkemper, S.K., Puschmann, D.U., Peth, S., Horn, R., 2014. Investigation of time

555   dependent development of soil structure and formation of macropore networks as

556   affected by various precrop species. Intern. Soil Water Cons. Res. 2, 51–66.

557   Pagliai, M., La Marca, M., Lucamante, G., Genovese, L., 1984. Effects of zero and

558   conventional tillage on the length and irregularity of elongated pores in a clay loam soil

559   under viticulture. Soil Tillage Res. 4, 433–444.

560   Passoni, S., Pires, L.F., Heck, R., Rosa, J.A., 2015. Three dimensional characterization

561   of soil macroporosity by X-ray microtomography. Rev. Bras. Ciência do Solo 39, 448–

562   457.

563   Pires, L.F., Borges, J.A.R., Bacchi, O.O.S., Reichardt, K., 2010. Twenty-five years of

564   computed tomography in soil physics: A literature review of the Brazilian contribution.

565   Soil Tillage Res. 110, 197–210.

566   Pires, L.F., Rosa, J.A., Timm, L.C., 2011. Comparação de métodos de medida da

567   densidade do solo. Acta Sci. Agron. 33, 161–170.

568   Pires, L.F., Borges, J.A.R., Rosa, J.A., Cooper, M., Heck, R., Passoni, S., Roque, W.L.,

569   2017. Soil structure changes induced by tillage systems. Soil Tillage Res. 165, 66–79.

570   Pires, L.F., 2018. Soil analysis using nuclear techniques: A literature review of the

571   gamma ray attenuation method. Soil Tillage Res. 184, 216–234.

572   Rasband, W., 2007. ImageJ.1997–2007. U.S.National Institutes of Health, Bethesda,

573   MD, USA.

574 Rezanezhad, F., Quinton, W.L., Price, J.S., Elrick, D., Elliot, T.R., Heck, R.J., 2009.
575   Examining the effect of pore size distribution and shape on flow through unsaturated
576   peat using computed tomography. Hydrol. Earth Syst. Sci. 13, 1993–2002.

577 Roque, W.L., Souza, A.C.A. de, Barbieri, D.X., 2009. The Euler-Poincaré characteristic
578   applied to identify low bone density from vertebral tomographic images. Rev. Bras.
579   Reumatol. 49, 140–52.

580 Roque, W.L., Arcaro, K., Alberich-Bayarri, A., 2012a. Tortuosity and elasticity study of
581   distal radius trabecular bone, in: Rocha, Á., Calvo-Manzano, J.A., Reis, L.P., Cota,
582   M.P. (Eds.), Sistemas Y Tecnologías de Información: Actas de La 7a Conferencia
583   Ibérica de Sistemas Y Tecnologías de Información. APPACDM – Associação
584   Portuguesa de Pais e Amigos do Cidadão Deficiente Mental, Madrid, pp. 1–4.

585 Roque, W.L., Arcaro, K., Lanfredi, R.B., 2012b. Trabecular network tortuosity and
586   connectivity of distal radius from microtomographic images. Brazilian J. Biomed. Eng.
587   28, 116–123.

588 Rossi, A.M., Hirmas, D.R., Graham, R.C., Sternberg, P.D., 2008. Bulk density
589   determination by automated three-dimensional laser scanning. Soil Sci. Soc. Am. J.
590   72, 1591–1593.

591 Russell, E.W., Balcerek, W., 1944. The determination of the volume and air space of soil
592   clods. J. Agric. Sci. 34, 123–132.

593 San José Martínez, F., Caniego, F.J., García-Gutiérrez, C., 2017. Lacunarity of soil
594   macropore space arrangement of CT images: Effect of soil management and depth.
595   Geoderma 287, 80–89.

596 Sander, T., Gerke, H.H., 2007. Noncontact shrinkage curve determination for soil clods
597   and aggregates by three-dimensional optical scanning. Soil Sci. Soc. Am. J. 71, 1448–
598   1454.

599 Schafer, W.M., Singer, M.J., 1976. Reinvestigation of effect of saran coatings on

600   extensibility of swelling soil clods. Soil Sci. 122, 360–364.

601 Schmitt, M., Halisch, M., Müller, C., Fernandes, C.P., 2016. Classification and

602   quantification of pore shapes in sandstone reservoir rocks with 3-D X-ray micro-

603   computed tomography. Solid Earth 7, 285–300.

604 Shipp, R.F., Matelski, R.P., 1965. Bulk-density and coarse-fragment determinations on

605   some Pennsylvania soils. Soil Sci. 99, 392–397.

606 Solgi, A., Naghdi, R., Labelle, E.R., Tsioras, P.A., Salehi, A., 2018. Comparison of

607   sampling methods used to evaluate forest soil bulk density. Croat. J. Eng. 39, 107–

608   114.

609 Staff, S.S., 2013. Simplified guide to soil taxonomy. USDA-Natural Resources

610   Conservation Service, National Soil Survey Center, Lincoln, USA.

611 Stewart, R.D., Abou Najm, M.R., Rupp, D.E., Selker, J.S., 2012. An image-based method

612   for determining bulk density and the soil shrinkage curve. Soil Sci. Soc. Am. J. 76,

613   1217–1221.

614 Timm, L.C., Pires, L.F., Reichardt, K., Roveratti, R., Oliveira, J.C.M., Bacchi, O.O.S.,

615   2005. Soil bulk density evaluation by conventional and nuclear methods. Aust. J. Soil

616   Res. 43, 97–103.

617 Toriwaki, J., Yonekura, T., 2002. Euler number and connectivity indexes of a three

618   dimensional digital picture. Forma 17, 183–209.

619 Tseng, C.L, Alves, M.C., Crestana, S., 2018. Quantifying physical and structural soil

620   properties using X-ray microtomography. Geoderma 318, 78–87.

621 Turner, W.R., Brown, D.S., Harrison, D.V., 1955. Properties of paraffin waxes:

622   composition by mass spectrometer analysis. Ind. Eng. Chem. 46, 1219–1226.

623 van Remortel, R.D., Shields, D.A., 1993. Comparison of clod and core methods for

624   determination of soil bulk density. Commun Soil Sci Plant Anal. 24, 2517–2528.

625 Vaz, C.M.P., de Maria, I.C., Lasso, P.O., Tuller, M., 2011. Evaluation of an advanced

626   benchtop micro-computed tomography system for quantifying porosities and pore-size

627   distributions of two Brazilian Oxisols. Soil Sci. Soc. Am. J. 75, 832–841.

628 Vogel, H.J., Kretzshmar, A., 1996. Topological characterization of pore space in soil –

629   sample preparation and digital image-processing. Geoderma 73, 23–38.

630 Zingg, T., 1935. Beitrag zur Schotteranalyse. Schweiz. Mineral. Petrogr. Mitt., 15, 39–

631   140.

Figure Captions

Figure 1. (a,b) Pictures of the sample coating with paraffin wax; (c) Picture of soil samples submitted to coating; (d) Paraffin wax inside one of the soil samples.

Figure 2. 3D images of one of the samples (S8) impregnated with paraffin wax. The three images on top represent the volume of pores, paraffin and solids, respectively. The graph presents the grey level histogram for one of the cross-sections analyzed. Arrows 1 to 4 indicate large and connected macropores close to the border of the sample.

Figure 3. Micromorphological characteristics of the soil samples. (a) Porosity (P); (b) Pore volume (PV); (c) Number of pores (NP); (d) Volumetric Euler-Poincare characteristic (EPC_V); (e) Tortuosity (τ); (f) Degree of anisotropy (DA).

Figure 4. (a) Normalized distributions of the mean porosity (P_N) in terms of different pore sizes; (b) Normalized distributions of the mean number of pores (NP_N) in terms of different pore sizes; (c) Normalized distributions of mean pore volume (PV_N) in terms of the shape of pores; (d) Normalized distributions of the mean number of pores (NP_N) in terms of the shape of pores; (e) Normalized distributions of mean pore volume (PV_N) in terms of the shape of pores not considering the non-classified pores; (f) Normalized distributions of the mean number of pores (NPN) in terms of the shape of pores not considering the non-classified pores. The results are presented for the whole soil porous system (■) and pores filled with paraffin wax (□). Bars indicate standard deviation of the mean. EQ: Equant; PR: Prolate; OB: Oblate; TR: Triaxial.
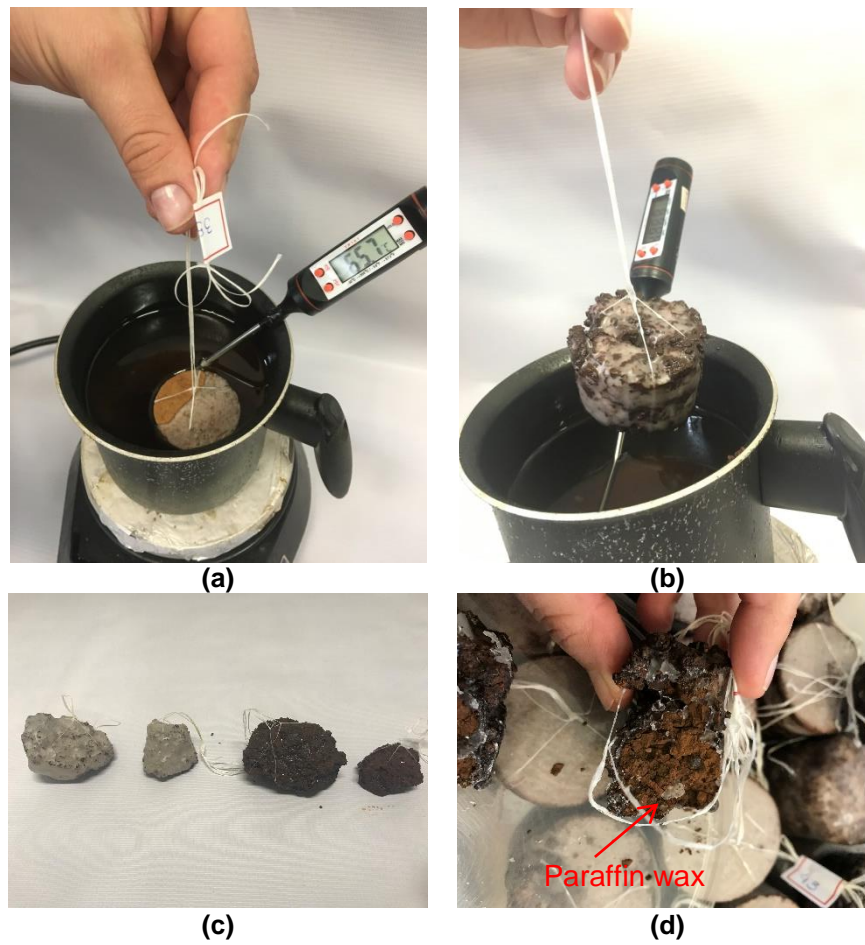
Figure 1. (a,b) Pictures of the sample coating with paraffin wax; (c) Picture of soil samples submitted to coating; (d) Paraffin wax inside one of the soil samples.
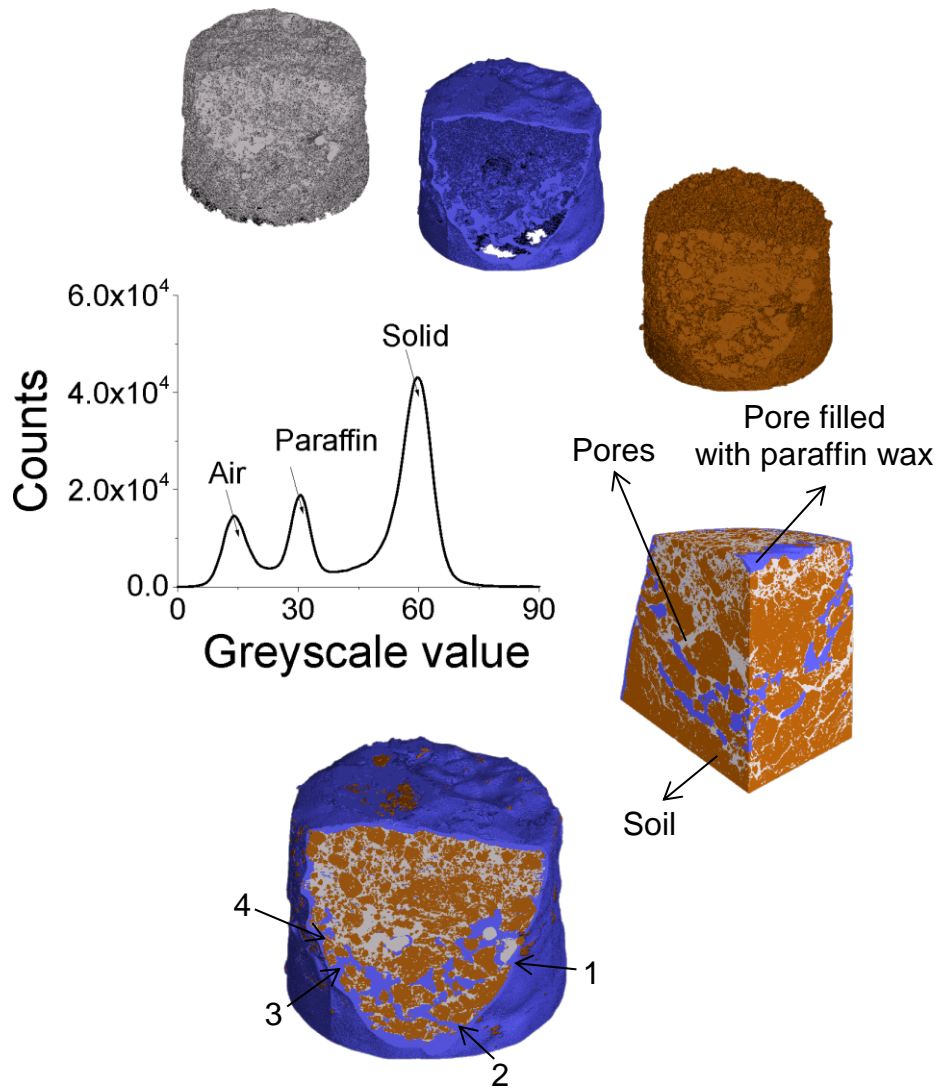
Figure 2. 3D images of one of the samples (S8) impregnated with paraffin wax. The three images on top represent the volume of pores, paraffin, and solids, respectively. The graph presents the grey level histogram for one of the cross-sections analyzed. Arrows 1 to 4 indicate large and connected macropores close to the border of the sample.
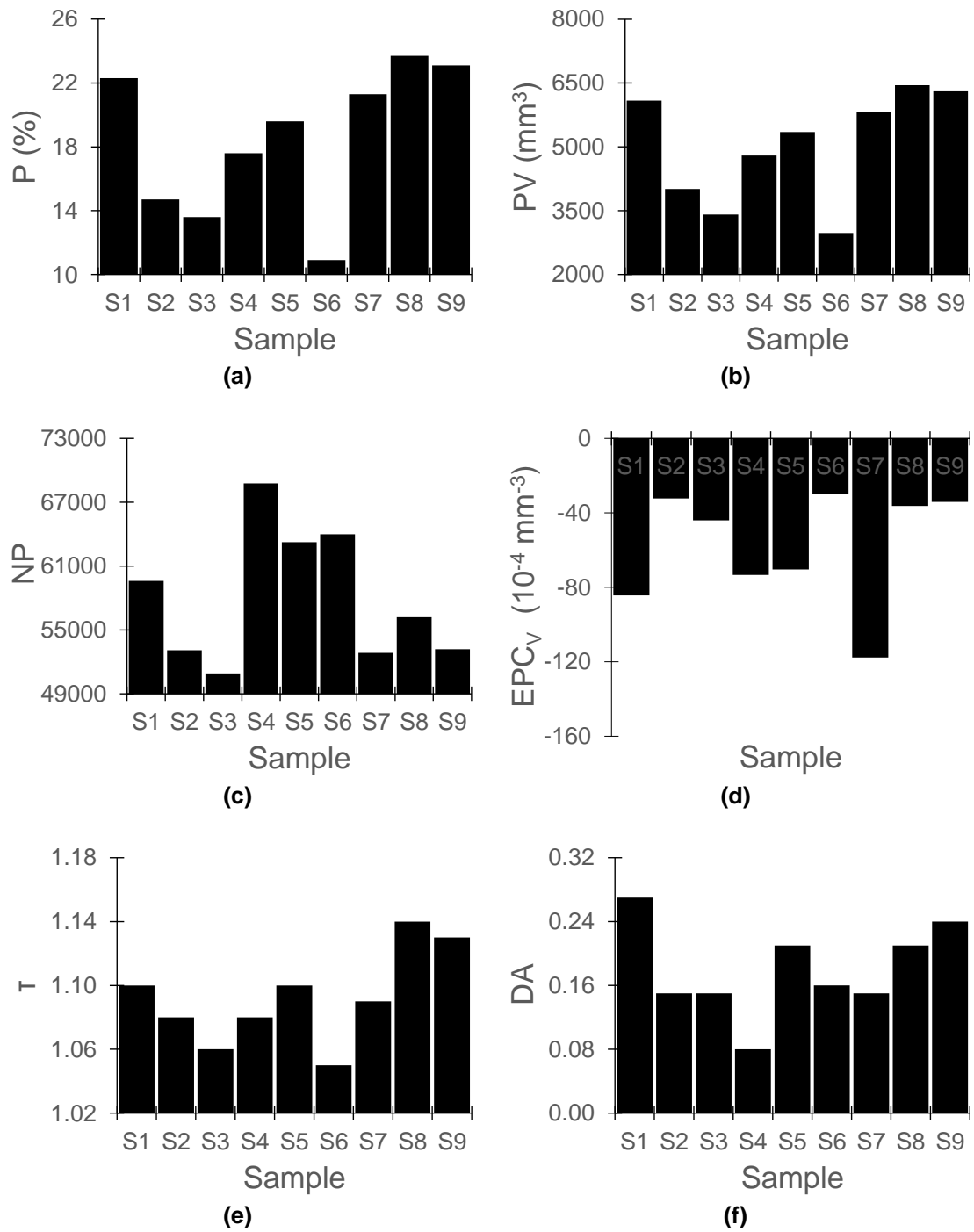
Figure 3. Micromorphological characteristics of the soil samples. (a) Porosity (P); (b) Pore volume (PV); (c) Number of pores (NP); (d) Volumetric Euler-Poincare characteristic (EPC_V); (e) Tortuosity (τ); (f) Degree of anisotropy (DA).
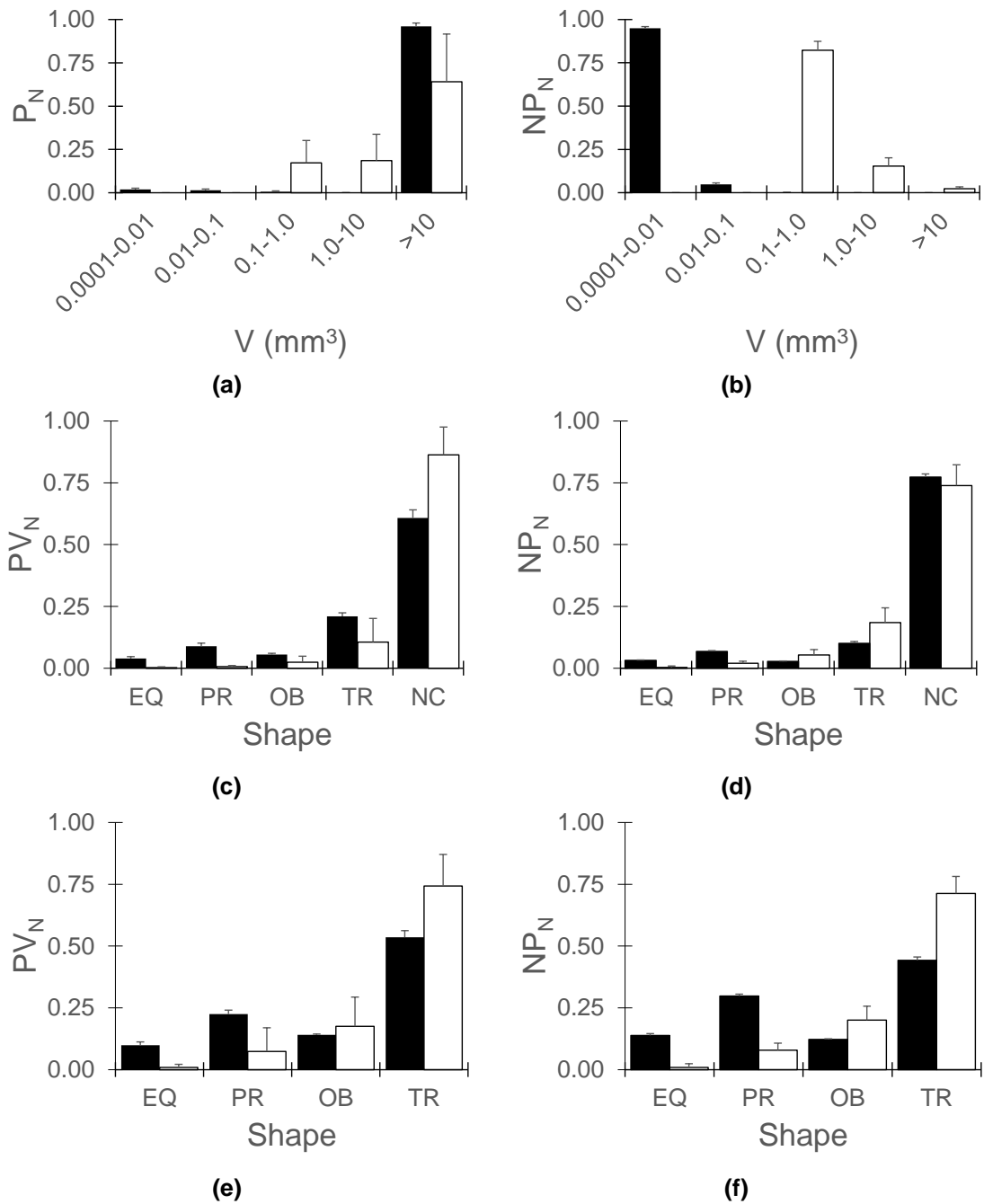
Figure 4. (a) Normalized distributions of the mean porosity (P_N) in terms of different pore sizes; (b) Normalized distributions of the mean number of pores (NP_N) in terms of different pore sizes; (c) Normalized distributions of mean pore volume (PV_N) in terms of the shape of pores; (d) Normalized distributions of the mean number of pores (NP_N) in terms of the shape of pores; (e) Normalized distributions of mean pore volume (PV_N) in terms of the shape of pores not considering the non-classified pores; (f) Normalized distributions of the mean number of pores (NPN) in terms of the shape of pores not considering the non-classified pores. The results are presented for the whole soil porous system (■) and pores filled with paraffin wax (□). Bars indicate standard deviation of the mean. EQ: Equant; PR: Prolate; OB: Oblate; TR: Triaxial.

Table 1. Pearson correlation coefficients among soil morphological parameters studied

Property	no.	1	2	3	4	5	6	7	8	9
PV (mm^3)	1	1.00								
P (%)	2	0.99**	1.00							
NP	3	-0.12	-0.16	1.00						
PaV (mm^3)	4	0.68*	0.68*	-0.04	1.00					
EPC$_V$	5	-0.38	-0.38	-0.12	0.31	1.00				
τ_{avg}	6	0.91**	0.91**	-0.20	0.87**	0.09	1.00			
DA	7	0.58	0.58	-0.25	0.67*	0.13	0.60	1.00		
EN$_B$	8	-0.40	-0.40	-0.41	0.18	0.45	-0.04	-0.07	1.00	
EN$_{>0.2}$	9	0.39	-0.39	-0.41	0.19	0.45	-0.04	-0.07	0.99**	1.00

PV (mm^3): pore volume; P(%): porosity; NP: number of pores; PaV (mm^3): paraffin wax volume; EPC$_V$: Volumetric Euler-Poincare Characteristic; τ_{avg}: average tortuosity; DA: degree of anisotropy; Th (mm): macropore thickness; EN$_B$: Euler number (largest pore); EN$_{>0.2}$: Euler number for pores larger than 0.2 mm^3; *, ** significantly different at p<0.05 and p<0.01

Table 2. Morphological characteristics of the soil porous system (whole sample) for pores larger than 0.2 mm^3

Sample	S1	S2	S3	S4	S5	S6	S7	S8	S9
PV$_{>0.2}$ (mm^3)	5953	3841	3252	4621	5193	2762	5673	6291	6148
P$_{>0.2}$ (%)	21.8	14.1	11.9	17.0	19.0	10.1	20.8	23.1	22.5
NP$_{>0.2}$	9	50	41	33	21	64	15	33	23
EN$_{>0.2}$*	-25	-9	-12	-21	-20	-9	-21	-11	-10

* All the values of EN$_{>0.2}$ presented should be multiplied for ×10^4

Table 3. Volume of pores occupied by paraffin wax in the region of interest studied

Sample	S1	S2	S3	S4	S5	S6	S7	S8	S9
P$_{pa}$ (%)	3.2	1.6	1.5	1.9	4.8	2.3	1.6	6.4	6.5
PaV (mm^3)	874	437	409	519	1310	628	437	1747	1774
% V$_o$	14.3	10.9	11.0	10.8	24.5	21.1	7.5	27.0	28.1

P$_{pa}$ (%): porosity considering pores occupied by paraffin wax; PaV: paraffin wax volume inside the samples; % V$_o$: percentage of the volume of pores occupied by the paraffin wax

Table 4. Morphological characteristics of the pores filled with paraffin wax larger than 0.2 mm^3

Sample	S1	S2	S3	S4	S5	S6	S7	S8	S9
P_{pa} (%)	1.9	1.1	0.7	0.8	3.9	1.6	0.9	6.1	6.2
PaV (mm^3)	510	286	180	227	1073	444	253	1671	1680
NP_{pa}	361	127	185	246	238	242	118	59	85

NP_{pa}: number of pores with paraffin

Table 5. Soil bulk density measured by the core and paraffin-coated methods

Sample type	No paraffin wax ingress	Paraffin wax ingress
	BD (g cm^{-3})	
Group 1*	1.30 a	1.41 b
Group 2**	1.24 a	1.33 b

* Group 1: clod samples; ** Group 2: samples collected in cylinders (core method) and removed from the cylinders for coating (paraffin-coated method); Means followed by same lower case letter were not significantly different (p≤0.05) in the comparison of BD for samples with and without paraffin wax ingress